*Journal of Testing and Evaluation*, Vol. 38, No. 5
Paper ID JTE102763
Available online at: www.astm.org

*S. Diego,*[1] *J. A. Casado,*[1] *I Carrascal,*[1] *J. A. Polanco,*[1] *and F. Gutiérrez-Solana*[1]

# Experimental Validation of an Adjustable Railway Fastening for Slab Track

**ABSTRACT:** A railway infrastructure capable of supporting a high frequency of light and heavy traffic, sometimes at high speed, requires the implementation of a high quality track. A correct definition of all track components leads to a high degree of safety and comfort for travelers as well as reduced operating costs. One factor that determines the elastic behaviour of the track is the rail fastening system. In this paper, the mechanical, electrical, and environmental sustainability characterization tests based on European standards UNE-EN have been carried out, verifying that the TK04 fastening system with a lateral adjustment of ±1 cm, manufactured by ThyssenKrupp Gleistechnik GmbH, satisfies the conditions and requirements of European standards UNE-EN for installation on slab track systems for light rail.

**KEYWORDS:** fastening, polyamide, clamping force, stiffness, longitudinal restraint, fatigue

## Introduction

Traditionally, the transversal track profile consisted of rails supported on sleepers arranged in a ballast layer, but the current trend provides the asphalt or concrete slab as a new way of settlement, replacing these materials in their role to ballast (see Fig. 1 [1]). The construction criteria are far more demanding than for conventional track when it comes to leveling, alignment, and rail gauge. The slab track offers significant advantages as regards ensuring the correct position of each of the elements that make it up, maintaining unchanged the geometric parameters through time. This type of structure requires less maintenance, which reduces operating time and thus increases the availability of the track. Another positive aspect is the improved security and reliability of its performance and repair before derailment, which is in principle less likely, as the slab track has two defenses: an active defense, which reduces the formation of cross-faults, resulting in a greater stability of the train, and a passive defense based on its robustness, which makes it stronger from the structural point of view. Additionally, it supports higher axle loads and transmits to the platform stresses, which are more evenly distributed tension and of a lower value than with ballast [2].

One of the essential constituent elements of this superstructure model is the rail fastening system to the concrete slab through the use of elastic fasteners whose main components are metal clips, insulating polymer plates, and bolts. These elements confine the foot rail and prevent longitudinal and lateral movements, as well as its rotation, because of the transverse, vertical, and longitudinal transmitted efforts by the wheels of vehicles. They also offer the flexibility required to counter the vertical wave movements of the track that would give rise to high dynamic forces between wheel and rail, thus avoiding vibration and noise. This system allows the positioning of the plan and elevation rail to be regulated, and it may correct any mounting faults or deviations due to any subsequent settlements [3,4].

Manuscript received October 9, 2009; accepted for publication February 16, 2010; published online March 2010.

[1]Dept. de Ciencia e Ingeniería del Terreno y los Materiales, E.T.S. Ingenieros de Caminos, Canales y Puertos, Univ. de Cantabria, Avda. Los Castros s/n, 39005 Santander, Spain, e-mail: jose.casado@unican.es

The slab track supports heavy and light transport transit, allowing the movement of high speed trains, trams, and subway. The aim of this study is to validate in terms of mechanical, electrical, and environmental sustainability the TK04 elastic rail fastening system with lateral adjustment to a ballastless light rail track on the basis of the tests and requirements of European standards UNE-EN [5–7]. For this, specifically developed procedures have been carried out to adapt the tests defined in the standard to the fastening object of this work.

## Material and Sample Preparation

The material under test is the TK04 fastening system with a lateral adjustment of ±1 cm manufactured by ThyssenKrupp Gleistechnik GmbH. This is an elastic fastening with direct attachment to the structure that improves the transmission of the rail efforts to the concrete. The components of this system are shown in Figs. 2 and 3. The UIC-54 type rail piece, which is mechanized in the wings of the foot to reduce its base from 140 to 125 mm and whose length is 500 mm, rests on a rail pad made of ethylene vinyl acetate copolymer whose dimensions are $(170/155 \times 123 \times 6)$ mm$^3$, which, in turn, is supported on a bed of polyamide six reinforced with 30 % glass fiber (PA6 GF30) based on a size of $(381 \times 150)$ mm$^2$. This whole set of elements is set on a stack of three additional plates, one

FIG. 1—*Example of slab track installed in Madrid subway [1].*

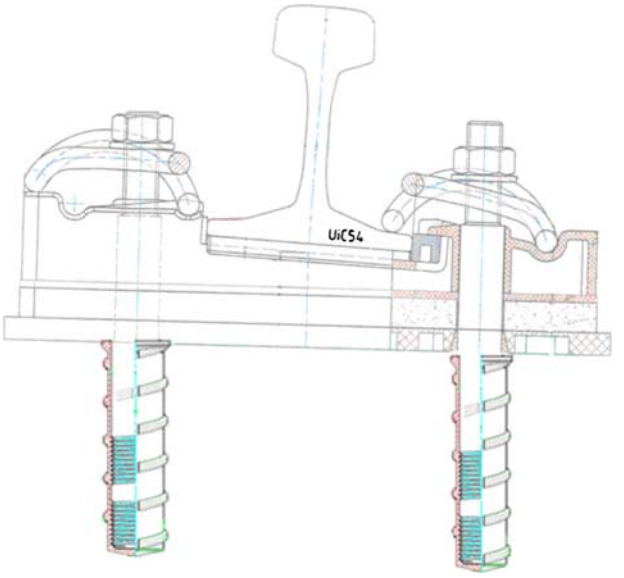


FIG. 2—*Scheme of the fastening system with lateral adjustment TK04 [4].*

of PA6 GF30 (384 × 154 × 5) $mm^3$, another of an intermediate porous thermoplastic-elastomer (384 × 154 × 20) $mm^3$, and another lower one embedded in the concrete of PA6 GF30 (402 × 172 × 3) $mm^3$. The set is fixed vertically by two metal clips type SKL-15 through galvanized screws (M30 × 250 mm) embedded in the concrete and sheathed in a PA6 GF30 sheathing. Two toothed wedges of PA6 GF30 are used to adjust sideways the rail seat in its support.

Several reinforced concrete blocks (500 × 300 × 200) $mm^3$ were produced with Minex Grout [8] to simulate the slab track support. In these blocks were embedded the screws and the bottom PA6 GF30 plate. Figure 4 shows the formwork and finishing of one of the blocks.

## Experimental Methodology and Equipment

The experimental techniques and the equipment used to carry out the characterization of the TK04 fastening system for slab track are now described. In all cases, tests were conducted at laboratory room temperature, between 18 and 22 °C.

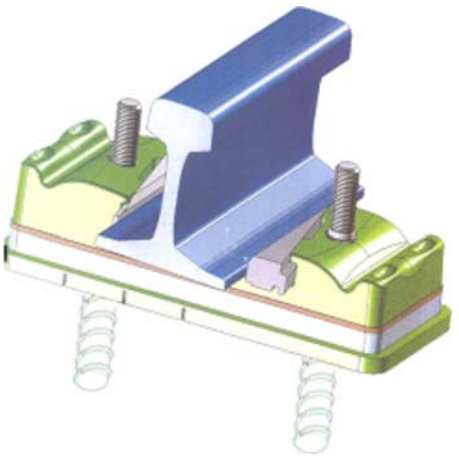

FIG. 3—*Components of the fastening system with lateral adjustment TK04 [4].*

FIG. 4—*Manufacture of concrete blocks. Side and top views.*

### *Dynamic Stiffness at Low Frequency ($K_d$)*

Given the polymeric nature of the materials that, stacked up, make up the support and rail fastening system, it is necessary to analyze their deformation response versus dynamic fluctuating efforts, which are those that are mostly present in its operating mode. Initially, each component is assembled to carry out its fastening by applying a torque of 180 N m with a FACOM brand, model S.325D torque wrench. The dynamic stiffness of the system, starting from the theoretical one declared by the manufacturer, between 75 and 100 kN/mm (considered as the worst condition), was verified by applying a cyclic compressive load (maximum force of $F_2$ = 55 kN and minimum force of $F_1$ = 5 kN) at 5 Hz for 1000 cycles, according to the specifications for a light rail track type [9]. A universal hydraulic testing machine with a load cell capacity of ±100 kN, INSTRON brand, and four linear variable differential transducers (LVDTs), SOLARTRON brand, with a range of ±5 mm were employed for the functional control, as shown in the photographs in Fig. 5. The experimental dynamic fastening system stiffness was determined by recording the last 100 loading cycles applied, transmitted by the rail to the fastening system, and the corresponding vertical displacement recorded by the LVDTs, according to expression 1, where $d_1$ and $d_2$ are averaged displacement values of the four sensors, corresponding to the extreme applied forces $F_1$ and $F_2$, respectively.

To test the tightening effect on the behaviour of the elastic fastening system, the test was repeated on a second occasion, without squeezing the system

$$K_d = \frac{F_1 - F_2}{d_1 - d_2} \ \text{(kN/mm)} \tag{1}$$

### *Longitudinal Rail Restraint*

This test is performed to ensure that the elastic fastening provides a longitudinal restraint effort of the rail and that it maintains it de-

FIG. 5—*Dynamic stiffness test at low frequency and detail of the LVDT's location.*

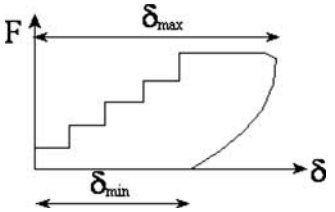


FIG. 6—*Diagram of longitudinal rail restraint test.*

spite the use, wear, fatigue, and vibrations due to the rail traffic. The rail fastening must also prevent the longitudinal displacement of the rail due to increases in temperature, must control the slip and separation of any gaps that may appear in the rail in case of breakage, and must not suffer translations or rotation induced by the rail if this tends to slide.

The system is fastening by applying a torque of 180 N m to each clip. The test consists in recording the tensile load and the corresponding longitudinal displacement of the rail applying and increasing load in increments of 2.5 kN at a rate of 10±5 kN/min, at constant intervals of 30 s between each step, until the longitudinal rail sliding with respect to the concrete block ($\delta_{max}$) is produced. In that instant the load is reduced to zero, and the rail displacement is continuously measured for 2 min more, recording the remaining slip ($\delta_{min}$). The measurement procedure is noted in the records of the applied force as a function of the rail sliding, as the diagram in Fig. 6 shows. The force corresponding to the difference between $\delta_{max}$ and $\delta_{min}(\Delta\delta)$, obtained from the curve, is noted as the longitudinal rail restraint value provided by the fastening system [5,10].

This cycle of loading and unloading is applied four times with a rest period of 3 min between each test; the first one is a system settlement. At no time must the components of the fastening system be adjusted. The Standard requires that the longitudinal rail restraint, the averaged value of the three tests after the initial seating, must be more than 7 kN.

The same testing machine as that described in the preceding paragraph was used to control the test functionally as well as an LVDT sensor with a range of ±5 mm in contact with the concrete block and subject to the rail base. The arrangement of the fastening elements in the test is illustrated in the photographs in Fig. 7.

## *Clamping Force Test*

Tightening is a basic parameter of the spring element of an elastic fastening system. It is defined as the vertical compressive force applied to the upper surface of the rail base by the fastening clips. The purpose of the test is therefore to verify the force transmitted by the spring element to the rail base. In service, the fastening must offer

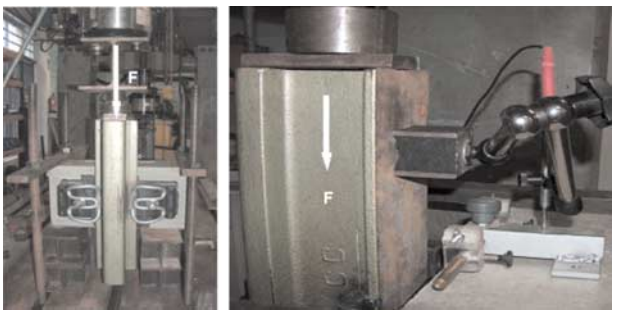


FIG. 7—*Longitudinal rail restraint test and detail of LVDT placement.*


FIG. 8—*Clamping force test. Detail of the gap between the foot rail and rail pad during the test.*

an elastic response to the relative movements between the rail and its support in the vertical direction, capable of tolerating the rail deflection and preventing it from lifting. In addition, it must maintain appropriate levels within the progression of the effort depending on the vertical displacement magnitude and provide a constraint between the rail and the other elements that make up its support.

The same test machine was used to conduct the test as well as four LVDT sensors with a range of ±5 mm in contact with the rail base and perpendicular to it, linked to the same concrete block previously tested with the arrangement shown in the photographs in Fig. 8.

An increasing tensile load is applied at a rate of 10 kN/min designed to produce the separation between the rail and the concrete block [6,11] through the rail piece. There is a continuous recording of data from the applied tensile load, $P$, and of the relative displacement between the concrete block and the rail obtained as the arithmetic mean of the reading made by the four comparators LVDT, δ. The rail pad is removed manually once the force required to produce the separation between the rail and the block has been reached. Then, the system is unloaded until the comparators record the initial test conditions, that is, the original rail position with respect to the block when the rail pad was placed in a seat is recovered at the load value $P_i$. Then it is discharged to a load value of $0.9P_i$, and then, the load is increased to a value of $1.1P_i$ at a rate of 10 kN/min. The $P_0$ value for $\delta=0$ (average of four comparators) is taken as the clamping force from the load-displacement diagram. The procedure is repeated twice more, and the average value of the clamping force is calculated.

## *Vertical Stiffness to 85 kN (K)*

Vertical elasticity within a range of loads from 80 to 100 kN can study the capacity of the support elements and rail fastening to ab-

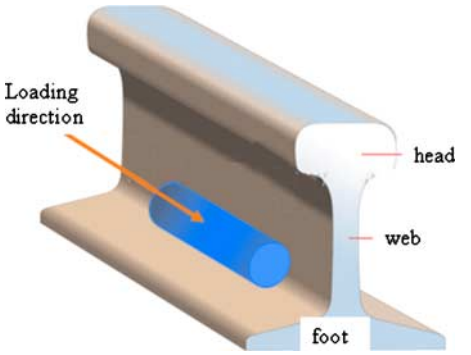


FIG. 9—*Welding of a bolt on modified rail type UIC-54 [7,12].*

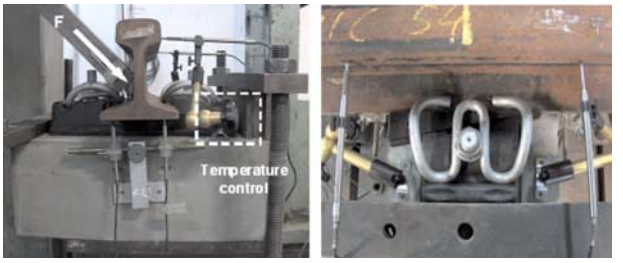


FIG. 10—*Dynamic inclined load test. Overview and detail of location of comparators.*

sorb vibrations and protect the slab track against the highest traffic loads. The same concrete block without any modification, test machine, and four displacement transducers with a range of ±5 mm were used for testing, with the provision shown in the photographs in Fig. 5. In this case, a set of six cycles of loading and unloading from 0.5 to 85 kN at a rate of 50 kN/min was applied, measuring at the sixth cycle the vertical rail displacement recorded as the average of four transducers. The force-displacement ratio (vertical stiffness $K$) of the set between 5 and 80 kN is calculated using the average rail displacement ($d$), according to expression 2 [5,9]

$$K = \frac{75}{d} \text{ (kN/mm)} \tag{2}$$

## *Repeated Loading (Dynamic Inclined Load)*

This test is performed to determine the long-term behaviour of direct rail fastening systems on the slab track. To accurately simulate the real efforts caused by the rail movement, it must be borne in mind that the more aggressive efforts occur both in straight sections, with the so-called whipping effect due to the convoy zigzag and in curved areas due to the action of centrifugal force. The generated impacts have a direction deflects from the vertical with an intensity and load angle that depend among other parameters on the track curvature radio (in the case of high speed rail, over 1000 m) and the stiffness of the rail pad. Therefore, the rail fastening must withstand the start-up effort without breaking or creep, avoid excessive track increase at curves, and resist excessive rollover of the rail (risk of derailment and wheel/rail wear), as well as having the required long-term fatigue strength. The dynamic inclined load test assesses the capacity of the whole fastening set subjected to prolonged fatigue caused by the effect of repeated loading in order to simulate the passage of the wheels on the rail.


FIG. 11—*Testing of embedded components device.*

The same test machine and six comparators were used for testing. The test consists of reproducing on the same concrete block previously tested a regular load of constant amplitude for 3 million cycles in a certain position and angle with respect to the head and the base of the piece rail, respectively [5,9]. The magnitude of the maximum load and the positioning of the effort applicators were determined from the dynamic stiffness at low frequency, $K_d$, of the whole fastening. In this case, considering a value of stiffness $K_d$ = 67.4 kN/mm (see Dynamic Stiffness at Low Frequency section) and a light railway track, we get the following test conditions: Angle of load application line of 45°, distance between load line and the bottom center of the rail head radius of 100 mm, and maximum compression load of 55 kN. To make the application load line pass through the point defined in the norm, it was made to coincide with the central axis of a bolt of 30 mm in diameter welded to the rail web (see diagram in Fig. 9)

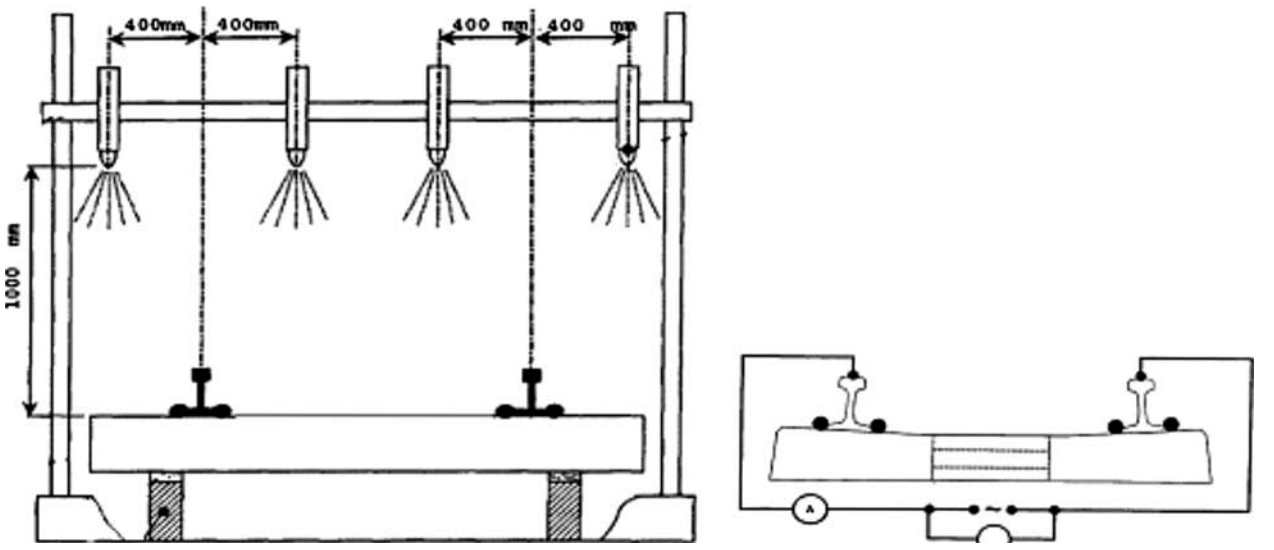


FIG. 12—*Test schematics. Watering device and electric installation.*

FIG. 13—*Electrical resistance test. General appearance and details of electrical connection.*

Once compliance with the initial conditions of the test is verified, a sinusoidal variable load is applied to the fastening set from a minimum load of 5 kN up to the maximum load for $3 \times 10^6$ cycles at a frequency of 5 Hz. The dynamic rail displacements relative to the concrete block are measured in the first and last 1000 cycles of the dynamic test, and they are compared for at least one cycle. The experimental design is shown in the photographs in Fig. 10.

The result is obtained by making a visual inspection of the various elements of the system and measuring the existing difference in relative displacements between the rail and the concrete block at the beginning and end of the $3 \times 10^6$ cycles to the minimum and maximum loads. The polymer temperature most strained mechanically in the vicinity of the rail was controlled during the test using a thermographic camera brand IRISYS 1011 (Fig. 10).

After this repeated load test, if there is no significant degradation or breakage of any component of the fastening system, the tests set out in sections Longitudinal Rail Restraint, Clamping Force Test, and Vertical Stiffness to 85 kN ($K$) are repeated to determine, through the difference in the results, the effects of fatigue on the system. The norm requires that the variation of results in the longitudinal rail restraint test is less than 20 %, the variation in the vertical stiffness is less than 25 %, and the variation in clamping force is kept below 20 %.

## *Embedded Fastening Components*

As a guarantee of security, the anchor element must remain fixed, embedded on the plate, to ensure a stable reference point to the other components of the fastening that act elastically. This stability must be maintained to perform the various operations involved in the assembly of the fastening and to resist the generated pulling out efforts during its service life.

FIG. 14—*Fastening system before exposure to salt fog.*

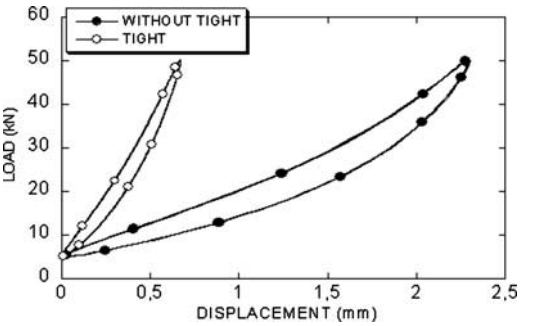


FIG. 15—*Determination of dynamic stiffness at low frequency.*

The fastening components that were embedded in the concrete block, after its hardening, were subjected to a vertical load testing of up to 60 kN at a speed of $50 \pm 10$ kN/min [5]. Once the value of 60 kN was reached, the load was maintained for 3 min to observe the state of the embedded components. After 3 min, the load was removed gently. The fastening of the concrete block was performed in accordance with the norm that establishes a radius of 100 mm from the tie-embedded component. Requirement [5] indicates that there should be no cracks visible, allowing only some exfoliation. The test configuration is shown in the photographs in Fig. 11. Subsequently, the pulling out of the embedded component in position control at a speed of 2 mm/min was performed. An actuator with a load cell, mark INSTRON 500 kN capacity, was used to run this test.

## *Electrical Resistance*

The fastening should provide an insulation of the track so as not to disturb the normal operation of electrical installations and signaling regardless of weather conditions. Electrical resistance testing is performed to verify the insulating properties of the fastening. The test setup requires the support of a concrete slab, specifically built to incorporate two fastening sets, in two electrically insulating supports not less than 50 mm thick [13]. The two complete fastening sets with two rail pieces of length 500 mm type UIC-54, clamped with a torque of 180 N m, were received with mortar in the concrete slab. Subsequently, a gate is positioned with an irrigation system in the vertical plane passing through the longitudinal axis of the plate with four nozzles situated at a height of 1000 mm from the top surface of the plate and separated by 400 mm from the plane of symmetry of the rail pieces, as shown in the diagram in Fig. 12.

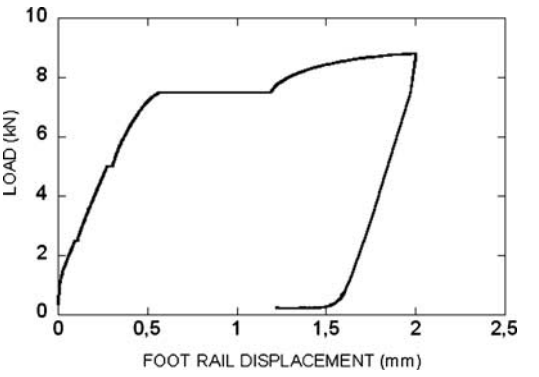


FIG. 16—*Rail load-slip.*

TABLE 1—*Longitudinal rail restraint.*

| Test | | $\delta_{max}$ (mm) | $\delta_{min}$ (mm) | $\delta_{max}-\delta_{min}$ (mm) | $F$ (kN) | $F_{average}$ (kN) |
|---|---|---|---|---|---|---|
| After | 1 | 2.00 | 1.22 | 0.78 | 7.50 | 7.50 |
| | 2 | 1.99 | 1.31 | 0.68 | 7.50 | |
| | 3 | 2.00 | 1.34 | 0.66 | 7.50 | |
| Before | 1 | 2.02 | 1.44 | 0.58 | 7.42 | 7.52 |
| | 2 | 2.06 | 1.50 | 0.56 | 7.51 | |
| | 3 | 2.03 | 1.43 | 0.60 | 7.62 | |

Then the rail pieces are connected to the electrical circuit that supplies 27 V ($V$) of alternating current (ac), as shown in the diagram in the same figure.

The system is sprinkled with water at a temperature between 10 and 20°C at a rate of 7±1 l/min by each injector for 2 min. The voltage and the intensity that circulate through the circuit are recorded during the spraying and at least 5 min after finishing it. The test is repeated two more times, leaving at least 24 h between them. The requirement is set at a value of electrical resistance greater than 5 kΩ. The actual device can be seen in the photograph in Fig. 13.

The calculation parameters in this test are the following:

- λ=correction factor used for the conductivity of the water;
- $R_\gamma$=minimum registered resistance, Ω;
- $R_C$=resistance corrected for the conductivity of water used, Ω; and
- γ=water conductivity used, mS/m.

The water comes from the public water supply, which has a measured conductivity, γ, of 36.5 mS/m, and therefore, correction factor λ=0,03 and γ=1,095 is applied [13]. The minimum electrical measured resistance on the sleeper is $R_\gamma$, while that required by the test is $R_C$, obtained from expression 3

$$R_C = \lambda x R_\gamma \ (\Omega) \tag{3}$$

Electrical resistance measures were made using a multimetre, FLUKE model 87, with an error of ±0.7 % of the voltage value and ±1.0 % in value of the intensity recorded. Also an output transformer with 27 V ac, brand POLILUX reference NC-63 (63 VA power), was used.

## *Effect of Severe Environmental Conditions*

The effects of exposure to harsh environmental conditions must be controlled, focusing on the corrosion of the metallic elements. Fastenings of the highest possible durability should be required, at least equal to that of the minimum rail and to the concrete slab for the anchor elements embedded in it, subject to an environment with adverse weather conditions: Ice, moisture, UV radiation, etc. The fastening system is subjected to the salt spray test to check the fastening resistance against the effects of extreme weather conditions. The methodology for testing the exposure of the fastening to severe environmental conditions has been established by the norm [5,14].

The fastening system mounted with a piece of rail was subjected to the effects of salt spray on the inside of a camera (see photograph in Fig. 14) with a NaCl concentration of 5 % by weight at a temperature of 35°C for 300 h [15]. After the test, the functionality of the system is verified, and once disassembled, the status of the various components is checked.

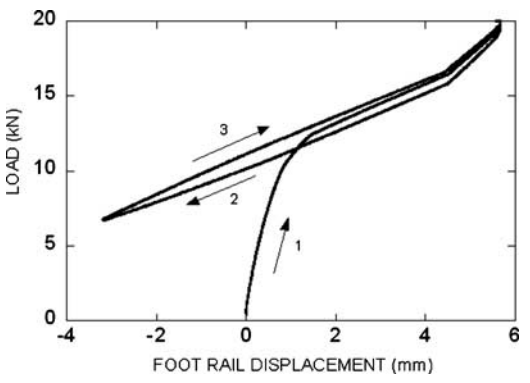


FIG. 17—*Load-displacement from the rail.*

## Results

### *Dynamic Stiffness at Low Frequency*

The graph in Fig. 15 shows the test result for dynamic stiffness at low frequency, with tight clips and without squeeze clips, representing for the final stages of testing the vertical descent of the support rail system with the applied force.

The dynamic stiffness values $K_d$ of 19.7 and 67.4 kN/mm were obtained for the fastening without squeezing and tightened with a torque of 180 N m, respectively.

### *Longitudinal Rail Restraint Test*

The characteristic fastening behaviour in this type of test, which shows the longitudinal rail restraint at each applied load step until its continued slip takes place, the immediate download, and its recovery ability, provided by both elastic metal clips, are presented in Fig. 16. Table 1 represents the longitudinal tensile effort, before and after the repeated loading test, applied on the rail and its corre-

TABLE 2—*Clamping force.*

| Test | | $F$ (kN) | $F_{average}$ (kN) |
|---|---|---|---|
| After | 1 | 12.27 | 12.35 |
| | 2 | 12.36 | |
| | 3 | 12.41 | |
| Before | 1 | 10.75 | 10.84 |
| | 2 | 11.13 | |
| | 3 | 10.63 | |

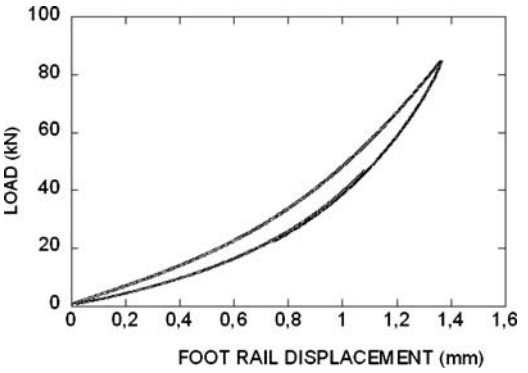


FIG. 18—*Load versus prior displacement.*

sponding slip over the concrete block. In each case, the test was repeated three times, after a pre-trial settlement, according to the norm.

Table 1 shows the maximum sliding ($\delta_{max}$) and residual ($\delta_{min}$) values of the rail with respect to the concrete block in each test and the corresponding longitudinal rail restraint, before and after the repeated load test, according to the established procedure.

The increase in sliding strength experienced after the repeated load fatigue test was 0.26 %.

## *Clamping Force Test*

The growing tensile effort that caused the vertical separation between the rail and the concrete block (indication 1) and the download that produces the vertical drop of the rail after the manual removal of the rail pad, which supported the rail foot (indication 2), are represented in Fig. 17. The tensile effort required to position the rail in its original position at the start of the test (indication 3), where the value of the clamping force is registered, can be seen. This test was repeated three times before and after the repeated loading test.

The clamping force values of the fastening prior to and after the repeated loading test obtained according to the established procedure are presented in Table 2.

The loss in clamping force after the fatigue test was 12.23 %.

## *Vertical Stiffness*

The evolution of the compressive load applied on the system in response to the mean displacement of the four comparators, for six cycles prior to the repeated loading test, is shown in Fig. 18.

The vertical stiffness obtained prior to the fatigue test was 64.43 kN/mm and that obtained after was 61.98 kN/mm, which is a loss rigidity of the system after the repeated loading test of 3.80 %.

## *Repeated Loading Strength (Dynamic Inclined Load)*

Once the test was finished, a visual inspection carried out on the fastening elements without disassembly revealed that they did not show signs of significant wear or damage. The measures taken as a control for monitoring the stiffness of the system at the beginning and end of the application of 3.000.000 load cycles on the whole of the fastening are reflected in Table 3, which shows the displacement of the rail with respect to the concrete block, measured with each of the six comparators.

From the table, it can be deduced that the rigidity of the fasten-

TABLE 3—*Measures of the dynamic inclined test.*

| | | Foot Rail[a] | | Head Rail[b] | |
|---|---|---|---|---|---|
| Fatigue Test | $F_{applied}$ | Displacement (mm) | Stiffness (kN/mm) | Displacement (mm) | Stiffness (kN/mm) |
| Initial | $F_{min}$ | 0.00 | 83.33 | 0.00 | 52.63 |
| | $F_{max}$ | 0.60 | | 0.95 | |
| Final | $F_{min}$ | 0.00 | 113.63 | 0.00 | 68.49 |
| | $F_{max}$ | 0.44 | | 0.73 | |
| Variation | $F_{min}$ | 0.00 | 30.30% | 0.00 | 15.86% |
| | $F_{max}$ | 0.16 | | 0.22 | |

[a]Average of four LVDTs.
[b]Average of two LVDTs.

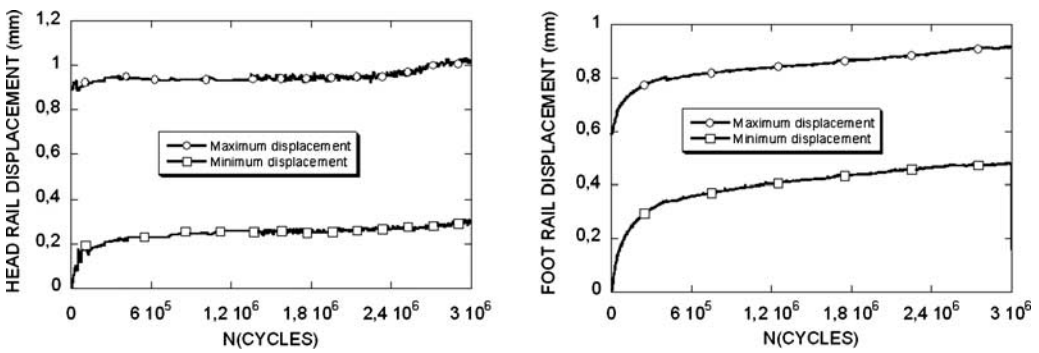


FIG. 19—*Head and foot displacement with respect to the concrete bock.*

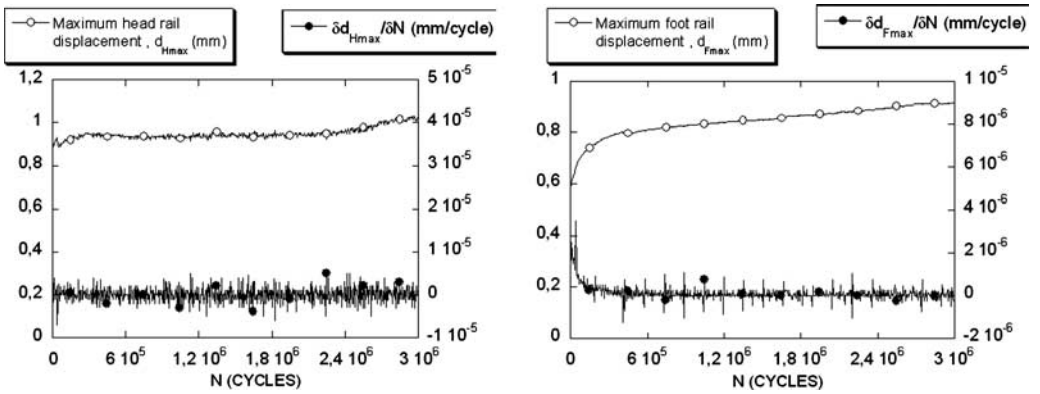


FIG. 20—*Displacement speeds of the head and foot with respect to the concrete block.*

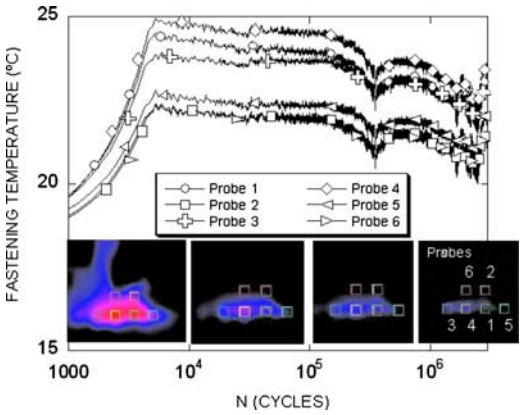


FIG. 21—*Evolution of the fastening temperature in critical areas during fatigue test.*

ing increases after the test by nearly 33 % (30 % at head and 36 % at foot) after accounting for a residual displacement of the head and the rail of 0.30 and 0.45 mm, respectively. These residual displacements are obtained from the evolution of the envelope wave displacement of the rail head and rail foot throughout the test and registered by the comparators that are represented in the diagrams in Fig. 19.

It can be seen that the above residual displacements to the minimum load of 5 kN at the head and foot are less than the allowable maximum of 1 and 0.5 mm, a condition in some technical specifications [16]. The derivatives of the functions of the maximum displacement of the head and the foot ($d_{H,\max}$ and $d_{F,\max}$) setting the speed of displacement experienced by these with the number of cycles are represented in the diagrams in Fig. 20. Thus, in both cases, speeds are determined in steady-state, small enough ($2.5 \times 10^{-7}$ and $5 \times 10^{-8}$ mm/cycle) not to produce the triggering processes of local damage or breakage in the material leading to system instability in the specific duration of this test [17].

These states of deformation are thermally conditioned by the thermoplastic nature of the materials [18]. The graph in Fig. 21 shows the evolution of surface temperatures of the most critical thermoplastic polymer areas of the fastening due to their greater susceptibility to warming associated to the effects of the dynamic loads applied. The record indicates that after the initial cycles of the test, the maximum temperature is reached at around 25 °C in the most stressed area and then stabilizes in all cases. Under these conditions, the polymeric fastening elements dissipate heat to the surroundings at the same speed at which it is generated by the friction between them and the internal molecular friction, denoting only slight fluctuations associated with changes in the temperature of the day and night. In any case the measured temperatures are below that of glass transition ($T_g$), which for the polyamide can be increased between 40 and 60 °C, depending on the humidity and the percentage of reinforcement of the polymer [19].

The evolution of elastic or stored energy ($E_S$) and the anelastic or energy dissipated ($E_D$) by the system throughout the test, as shown in the graphs in Fig. 22, can be determined from the records of the full-wave signals of the applied force and the corresponding relative displacement of the head and base of the rail with respect to the block. There is a stabilization of the energy values, more uniform in the case of the rail foot, consistent with the observed thermal constancy.

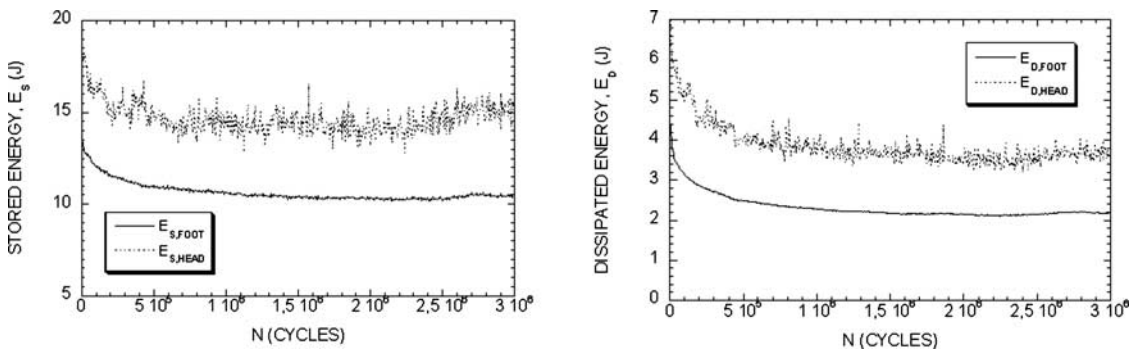


FIG. 22—*Stored and dissipated energy per cycle.*

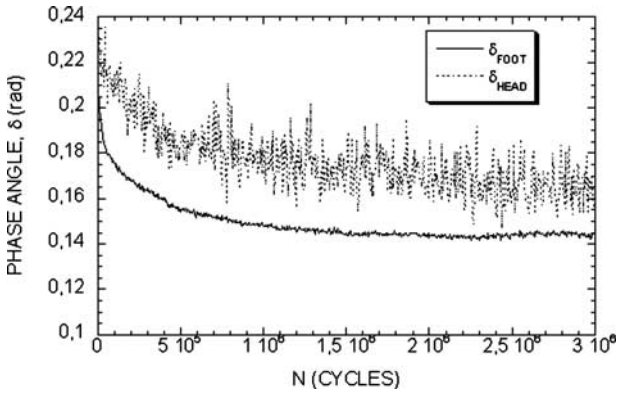


FIG. 23—*Phase angle.*

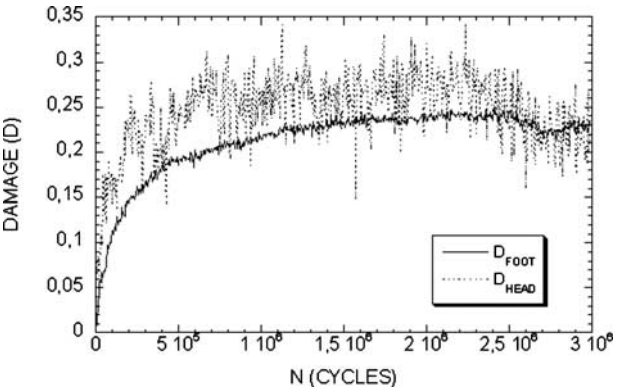


FIG. 24—*Damage evolution.*

From a thermoplastic material [20], viscoelastic parameters can be obtained as the phase angle (δ) between the sinusoidal signals of the applied force and the displacement undergone from the measurements made according to energy expression 4 [21], where $F_m$ represents the mean value of the wave force and its amplitude $F_0$. The graph in Fig. 23 shows the evolution of the calculated phase angle, which shows no characteristic peaks corresponding to movements of local or generalized chain segments such as those that would have been detected if the value of $T_g$ had been reached. This reconfirms the integrity of the system throughout the test [22]

$$tg\,\delta = \frac{4 \cdot F_m \cdot \dfrac{E_D}{E_S}}{\pi \cdot F_0 \cdot \left(2 + \dfrac{E_D}{E_S}\right)} \tag{4}$$

A further damage parameter, $D$, can be defined, representing the degree of material deterioration. Traditionally the formulation on the damage is based on the concept of equivalent stress and strain [23,24], assuming an effective stress experienced by the material due to the change in net section through the different mechanisms of damage. The damage, $D$, can be defined from the following expression:

$$D = 1 - \frac{E_N}{E_0} \tag{5}$$

where $E_0$ is the elastic modulus of the material without damage and $E_N$ is the apparent modulus in the form of material damage.

Given the proportionality between the elastic modulus, defined from the storage module and loss module [25], and the stored and dissipated energies determined in the test, the two parameters can be related. To determine the damage throughout the fatigue test, the energy stored, $E_{SN}$, rather than the energy dissipated, was chosen as a parameter to be assessed, as the results of the latter are less stable. The damage along the load cycles is defined as $D$ (N) according to expression 6 adapted to conditions of compressive loading, where $E_{S0}$ is the energy dissipated in the first cycle. The evolution of the damage parameter is shown in Fig. 24

$$D(N) = 1 - \frac{E_{SN}}{E_{S0}} \tag{6}$$

To be able to set a critical value of damage ($D_C$), it would be necessary to perform a more demanding dynamic load test on the whole of the fastening in order to produce its fracture to determine the critical energy relations that define this parameter. However, a functionality limit can be set for the fastening system from a readily controllable parameter as is the gauge. Assuming a maximum permissible range, as defined for the Madrid subway at 2 mm [26] (determined from the horizontal movement of the rail head), a total limit life of the fastening can be established from the displacement speed of the rail head previously measured ($2.5 \times 10^{-7}$ mm/cycle) based on its tolerance of 8 million cycles.

## *Embedded Fastener Components*

Figure 25 shows the test results for vertical load on the embedded elements and the subsequent pulling out test on the concrete block.

After the vertical load test to 60 kN on the embedded elements, given the layout of the plate embedded in the concrete block, no visible cracks or faults could be observed in the vicinity of the screw. However, the appearance of two cracks (not directed towards the screw) on the concrete block could be appreciated. Then, once the system was disassembled, the pulling out resistance was tested. The block started to fracture from cracks caused earlier and broke under an applied load of over 73 kN. In any case, the results of these tests are heavily influenced by the type of frame used and its place inside the concrete block.

## *Electrical Resistance*

The values of the electrical resistance of the system, taken 2 min after watering, $R_\gamma$, are shown in Table 4 for an applied voltage of $V$=27 V ac, as well as the values of electrical corrected resistance for the water conductivity, $R_C$ yielding a value of 82.0 kΩ.

## *Effects of Severe Environmental Conditions*

The first saline deposits with white oxides of zinc from the clips and red iron oxides from the rail and screws appeared 22 h after starting the test. At 49 h, corrosion products from the screws were detected. At 163 h, a widespread corrosion of the screws, nuts, and washers was detected, plus a growing red corrosion in the clips. The overall aspect of the fastening after the 300 h of testing required is shown in the photographs in Fig. 26.

After disassembly and cleaning of the elements of the fastening to remove the salt deposits, the polymer components did not show any damage due to the aggressive environment. Only the thermoplastic-elastomer porous elastic plate shows a permanent

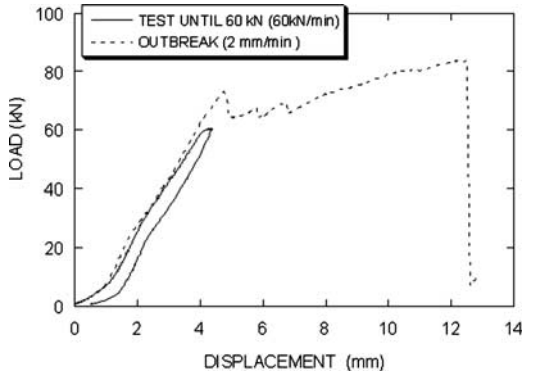


FIG. 25—*Vertical load and pulling out test.*

TABLE 4—*Results of electrical resistance test.*

| Test | $R_\gamma$ (kΩ) | $R_C$ (kΩ) |
|---|---|---|
| 1 | 73.60 | 80.59 |
| 2 | 82.12 | 89.92 |
| 3 | 69.77 | 76.40 |

FIG. 26—*Ambiental damage evolution.*

deformation due to the crushing occurring in the application of torque. Corrosion was observed widespread across the red surface of the screws, nuts, and washers. On the surface of the clip extends white corrosion due to the zinc of galvanized and red corrosion due to the steel. In any case the functionality was correct.

## Conclusions

The fastening system with lateral adjustment TK04 manufactured by ThyssenKrupp Gleistechnik GFT GmbH has not suffered fractures or signs of wear or tear of its components after the tests performed in this study and satisfies the requirements of European standard UNE-EN 13481-5:2003 on the performance requirements for fastening systems for slab track.

It has been shown that the thermoplastic components of the fastening and particularly the most stressed one of reinforced polyamide—in response to the fatigue test with the parameters of variation of load, angle of solicitation, frequency, and number of cycles used—which condition its behaviour and wear in later service, maintain a stable temperature, much lower than that of its glass transition. Under these conditions, all the cumulative effects of damage on the polymer material of the fastening would be of the mechanical type and slow enough to provide a far longer fatigue life than that required.

## *Acknowledgments*

The writers of this paper wish to express their sincere gratitude to the company ThyssenKrupp GFT Gleistechnik GmbH for supplying the necessary material and documentation to perform the work. Appreciation is extended to the company CETREN Certification for tracking the progress of the tests.

## References

[1] Adrover, B., 2008, “La Implementación de la vía en Placa en Líneas con Balasto en Explotación Comercial [The Implementation of Slab Track in Lines with Ballast of Commercial Exploitation],” Ph.D. thesis, Universidad Politécnica de Cataluña, (Vías y Construcciones, S.A.).

[2] Hernando, A., “La vía en Placa [The Slab Track],” *Report No. 24* , Artículos y Reportajes de FCMAF, Federación Castellano Manchega de Amigos del Ferrocarril, 2005.

[3] Escolano, J., “La vía en Placa en la DB AG [Slab Track in DB AG],” *Revista de Obras Públicas.* 145 (3382), Colegio de Caminos, Canales y Puertos, Santander, Spain, 1998, pp. 21–34.

[4] THYSSENKRUPP, “Sujeción de Carril con Apoyo Elástico y Aislamiento Eléctrico para vía en Placa [Rail Fastening with Elastic Pad and Electrical Insulation for Slab Track],” *Informe Técnico, Report No. 3*, Ingenieurbüro Führer, Dresden, 2004.

[5] UNE-EN 13481-2:2003, 2003, “Railway Applications. Track. Performance Requirements for Fastening Systems. Part 2: Fastenings Systems for Concrete Sleepers,” The European Committee for Standardization, Brussels.

[6] UNE–EN 13481–5:2003, 2003, “Railway Applications. Track. Performance Requirements for Fastening Systems. Part 5: Fastenings Systems for Slab Track,” The European Committee for Standardization, Brussels.

[7] UNE-EN 13481-6:2003, 2003, “Railway Applications. Track. Performance Requirements for Fastening Systems. Part 6: Special Fastening Systems for Attenuation of Vibration,” The European Committee for Standardization, Brussels.

[8] MINEX-SYSTEME TECHNIK GMBH, Industriestrasse 1 26452 Sande. Niedersachsen, Bundesrepublik, Deutschland.

[9] UNE-EN 13146-4:2003, 2003, “Railway Applications. Track. Test Methods for Fastening Systems. Part 4: Effect of Repeated Loading,” The European Committee for Standardization, Brussels.

[10] UNE-EN 13146-1:2003, 2003, “Railway Applications. Track. Test Methods for Fastening Systems. Part 1: Determination of Longitudinal Rail Restraint,” The European Committee for Standardization, Brussels.

[11] UNE-EN 13146-7:2003, 2003, “Railway Applications. Track. Test Methods for Fastening Systems. Part 7: Determination of Clamping Force,” The European Committee for Standardization, Brussels.

[12] N.R.V. 3-0-0.0, 1981, “Carriles. Barras Elementales [Rails, Elementary Bars],” Dirección Técnica, Mantenimiento de Infraestructuras de RENFE, Madrid, Spain, Primera Edición.

[13] UNE-EN 13146-5:2003, 2003, “Railway Applications. Track.

Test methods for fastening systems. Part 5: Determination of Electrical Resistance," The European Committee for Standardization, Brussels.

[14] UNE-EN 13146-6:2003, 2003, "Railway Applications. Track. Test Methods for Fastening Systems. Part 6: Effect of Severe Environmental Conditions," The European Committee for Standardization, Brussels.

[15] ASTM B117-07a, 2007, "Standard Practice for Operating Salt Spray (Fog)," *Annual Book of ASTM Standards*, Vol. 03.02, ASTM International, West Conshohocken, PA.

[16] Gestor de Infraestructuras Ferroviarias, *Pliego de Bases para el Suministro de Sujeciones*, Technical Standard, Madrid, Spain, 1999.

[17] Casado, J. A., 2003, "Comportamiento en Fatiga de Poliamidas Reforzadas con Fibra de Vidrio [Fatigue Behaviour of Fiber-Glass Reinforced Polyamides]," Ph.D. thesis, Universidad de Cantabria, Santander, Spain.

[18] Aharoni, S. M., *n-Nylons: Their Synthesis, Structure and Properties*, John Wiley & Sons, New York, 1997, ISBN: 978-0-471-96068-3.

[19] Murthy, N. S., "Glass Transition Temperature and the Nature of the Amorphous Phase in Semicrystalline Polymers: Effects of Drawing, Annealing and Hydration in Polyamide 6," *Int. J. Polym. Mater.*, Vol. 50, No. 3–4, 2001, pp. 429–444.

[20] Carrascal, I., Casado, J., Polanco, J., and Gutiérrez-Solana, F., *Análisis Dinamo-Mecánico Macroscópico (M-DMA) Sobre Componentes Estructurales de Poliamida 6.6 Reforzada con Fibra de Vidrio Corta [Macroscopic Dynamic-Mechanical Analysis on Structural Components of Short-Fiber-Glass Reinforced Polyamide 6.6]*, Asociación Española de Materiales Compuestos (AEMAC), Zaragoza, 2003, pp. 543–551.

[21] Carrascal, I., Casado, J., Varona, J., Polanco, J., and Gutiérrez-Solana, F., "Determinación del Fallo por Fatiga en Base a Consideraciones Energéticas de Componentes de Poliamida 6.6 Reforzada con Fibra de Vidrio [Fatigue Damage Determination Based on Energetic Considerations of Glass Fiber Reinforced Polyamide 6.6 Components]," *Anales de Mecánica de la Fractura*, Vol. 21, 2004, pp. 427–431.

[22] Kinloch, A. and Young, R. J., *Fracture Behaviour of Polymers*, Elsevier Applied Science, London, 1990.

[23] Jessen, S. and Plumtree, A., "Continuum Damage Mechanics Applied to Cyclic Behaviour of a Glass Fibre Composites Pultrusion," *Composites*, Vol. 22, No. 3, 1991, pp. 181–190.

[24] Sullivan, R. W., "Development of a Viscoelastic Continuum Damage Model for Cyclic Loading," *Mech. Time-Depend. Mater.*, Vol. 12, No. 4, 2008, pp. 329–342.

[25] UNE-EN ISO 6721-1, 2001, "Plastics. Determination of Dynamic Mechanical Properties. Part 1: General Principles," The European Committee for Standardization, Brussels.

[26] MM-EV-1-2-01, 2005, "Especificación de vía "Fabricación y Homologación de vía en Placa con Tacos Prefabricados Embebidos en Elastómero [Railway Technical Specification, Manufacturing and Certification of Dies for Slab Track Embebed in Elastomer]," Documento Metro Madrid, Madrid, Spain, Edición 1.